BRILL

IAWA Journal 42 (2), 2021: 191–203

iawa

Sperry's packing rule affects the spatial proximity but not clustering of xylem conduits: the case of *Fagus sylvatica* L.

Angelo Rita[1,*], **Osvaldo Pericolo**[1], **Antonio Saracino**[2], and **Marco Borghetti**[1]

[1]Scuola di Scienze Agrarie, Forestali, Alimentari e Ambientali, Università della Basilicata, Viale dell'Ateneo Lucano 10, 85100 Potenza, Italy

[2]Dipartimento di Agraria, Università di Napoli Federico II, via Università 100, 80055 Portici (Naples), Italy

*Corresponding author; email: angelo.rita@unibas.it

Accepted for publication: 25 June 2020

ABSTRACT

Sperry's packing rule predicts the optimum packing of xylem conduits in woody plants, where the frequency of xylem conduits varies approximately inversely with the square of the conduit radius. However, it is well established that such anatomical disposition does not remain fixed but is subject to a suite of adaptations induced by physiological constraints driven by both ontogenetic development and environmental characteristics. Here we challenge the hypothesis that increasing frequency of xylem conduits, concomitant with the decrease in their lumen area along the xylem pathway, would affect the spatial distribution of vessels inside tree-rings and their aggregation. To this end, we measured the vessels' anatomical characteristics inside each tree-ring along with a complete radial series taken at different stem heights of *Fagus sylvatica* L. trees. Point pattern analysis indicated a significant effect of the distance from the tree base and a weak effect of cambial age on the nearest neighbour distance among xylem vessels, suggesting that vessels were closer to each other near the apex, and became progressively more distant toward the base. The spatial pattern of xylem vessels violated the assumption of complete spatial randomness, vessel spatial arrangement followed a uniform distribution at different distances from the tree base. Although there was an increase in the intensity and proximity among vessels, we demonstrated that no patterns of aggregation between vessels were found in sampled *F. sylvatica* trees. Rather, point pattern profiles clearly highlighted a lack of aggregation of vessels in the face of a regular spatial distribution in the annual growth rings along the stems.

Keywords: Wood anatomy; axial packing; point pattern analysis; tapering; xylem network; water transport; vessel grouping.

INTRODUCTION

The soil-plant-atmosphere hydraulic transport via the xylem network is at the heart of all terrestrial plant growth and development (Ryan *et al.* 2006; Savage *et al.* 2016; Anderegg *et al.* 2018). To date, our knowledge of the hydraulic architecture of trees has been much improved and has allowed for a much more realistic and comprehensive vision of tree-water relationships. In this sense, xylem structure is conceived as a complex vascular network, which simultaneously fulfills the needs of water transport, mechanical support, and nutrient storage (Hacke & Sperry 2001; Tyree & Zimmermann 2002).

Long-distance water flow in angiosperms occurs through the lumens of vessel elements stacked end-to-end and interconnected at the end walls and through the lateral pits. Because vessels are of finite length, water can move from vessel to vessel through lateral inter-conduit pitting (determined by the density and size of the pit membranes), which, in addition to the number of conduits, defines the connectivity of the xylem network. It follows that the function of a tree's hydraulic system is largely determined by the frequency, diameter, and length of conduits within the xylem network from roots to leaves, resulting in a trade-off between hydraulic safety and efficiency (Sperry *et al.* 2008; Savage *et al.* 2010). Inter- and intraspecific xylem anatomical designs have been demonstrated to represent functional adaptations to increasing tree size (Anfodillo *et al.* 2006), as well as environmental constraints such as variation in water availability (Rita *et al.* 2015; Castagneri *et al.* 2019; González-Cásares *et al.* 2019).

Within individual trees, the largest vessels are found in roots, from where vessel lumen diameters become acropetally tapered. Small conduits tend to be distributed in distal parts of trees, such as the apical positions (Anfodillo *et al.* 2006; Petit

Published by Koninklijke Brill NV, Leiden

DOI 10.1163/22941932-bja10036

et al. 2010). In this way, tapered vessels minimize the build-up of resistance with tree size because of the increasing path length by maintaining similar conductivity with an increase in the number of xylem vessels per unit of cross-sectional area. To date, our understanding of xylem hydraulic properties has improved with the development of fractal-like tree models (West *et al.* 1999; Anfodillo *et al.* 2006; Savage *et al.* 2010) and novel experimental tools to visualize the cross-sectional and three-dimensional structure of xylem (Page *et al.* 2011; von Arx *et al.* 2016).

Among others, the structural model of the hydraulic transport system proposed by West, Brown, and Enquist (WBE) (West *et al.* 1999), which assumes that plants minimize the effect of hydrodynamic resistance imposed by increasing height by tapering the xylem conduits, has been widely used to explain the maintenance of a constant flow rate along the entire flow path. Although the WBE model proved useful to explain observed patterns of branching and hydraulic conductivity in vascular systems it does not appear to fully describe the trade-offs between efficiency and hydraulic safety that has shaped the evolution of vascular networks (Savage *et al.* 2010). These authors showed that a model based on optimal space-filling and a general "packing rule" (*sensu* Sperry *et al.* 2008), where the frequency of xylem conduits varies approximately inversely with the square of the conduit radius, accounts for the xylem variation in a wide range of plants. This "rule" contradicts the WBE assumption that conduit frequency remains constant as conduits taper and leads to a prediction of a constant total conduit area at each level of branching and better fits the majority of anatomical observations in the literature. In this regard, the packing function represents a cornerstone of a robust framework for modeling the xylem transport network (Sperry *et al.* 2008; McCulloh *et al.* 2010).

Although these mathematical models of xylem trait variability across plants provide an important description of xylem networks and helped us to determine whole-plant conductance and vulnerability better than simpler lumped models, such as Ohm's analogy, a rather limited amount of information on vertical variation in hydraulic traits and allometry currently limits advances in this direction (Mencuccini *et al.* 2019). That is, one questions whether the increasing pattern in the frequency of the vessels concomitant with the decrease in their average lumen size along the stem described by the "packing rule" produces increased spatial "proximity" among vessels and clustered vessels (groups of three or more vessels having both radial and tangential contact; IAWA Committee 1989) because of the reduced space. To address this question, the spatial distribution of xylem conduits in the whole tree, where aspects related to the tapering/packing of xylem conduits become relevant needs to be examined. This may allow us to (i) gain new insight into the general pattern predicted by the models, (ii) improve our capability to model water fluxes in plants and (iii) better clarify both the mechanisms involved, as well as the possible physiological and ecological trade-offs, as also suggested by Martínez-Vilalta *et al.* (2012) and Mencuccini *et al.* (2010, 2019).

Traditionally, rather little attention has been paid to the spatial distribution of vessels and their possible role in the hydraulic plant system. Earlier works based on connectivity among vessels reported that they are usually randomly arranged (Zimmermann & Jeje 1981; Tyree & Zimmermann 2002) except near nodes and leaf abscission zones (André *et al.* 1999). More recently, attention to intervessel connectivity has increased because of ecological differences in vessel arrangement between closely related species (Carlquist 2009; Mencuccini *et al.* 2010; Lens *et al.* 2011), such as the rare-pit hypothesis (Wheeler *et al.* 2005; Lens *et al.* 2011), ion-induced increase in hydraulic conductivity (Jansen *et al.* 2011; Nardini *et al.* 2012), and safety-efficiency tradeoffs (Loepfe *et al.* 2007; Martínez-Vilalta *et al.* 2012), although the controversy regarding the functional role of vessel grouping is yet not clarified. In this regard, vessel grouping has been demonstrated to be an adjustment by several tree species frequently associated with particular ecological environments or stressful conditions (Robert *et al.* 2009; Lens *et al.* 2011; von Arx *et al.* 2013; Schuldt *et al.* 2016). For example, a higher degree of grouping is attained by fewer solitary vessels and larger groups of vessel multiples in trees growing either in arid or cold habitats (Carlquist 1984; Baas & Carlquist 1985; von Arx *et al.* 2013).

However, although many of the aforementioned studies have long highlighted the large variation in vessel grouping across woody angiosperms and within particular families, the ontogenetic influence on the xylem vessel spatial pattern, namely the finding that conduit spatial distribution can be affected by conduit density, remains poorly explored.

In this study, we investigated the spatial distribution of vessels (either grouping or vessel isolation) according to the axial and radial development of trees. We challenge the hypothesis that the increased frequency of xylem vessels, concomitant with the decrease in their lumen area along path length, as predicted by the "packing rule," would affect vessel aggregation (groups built into larger patterns, Carlquist 1984) merely because of packing (Fig. 1). Alternatively, we suggest that properties related to vessel clustering more likely have a functional significance, mostly related to hydraulic adjustments in response to environmental constraints over a plant's lifetime, rather than a simple lumped mechanistic explanation. To this end, for a common time span, we measured tree-ring vessel characteristics, including their spatial arrangement (cartesian coordinates), in stem discs collected at different points along the axial pathway from eight *Fagus sylvatica* L. trees, one of the most

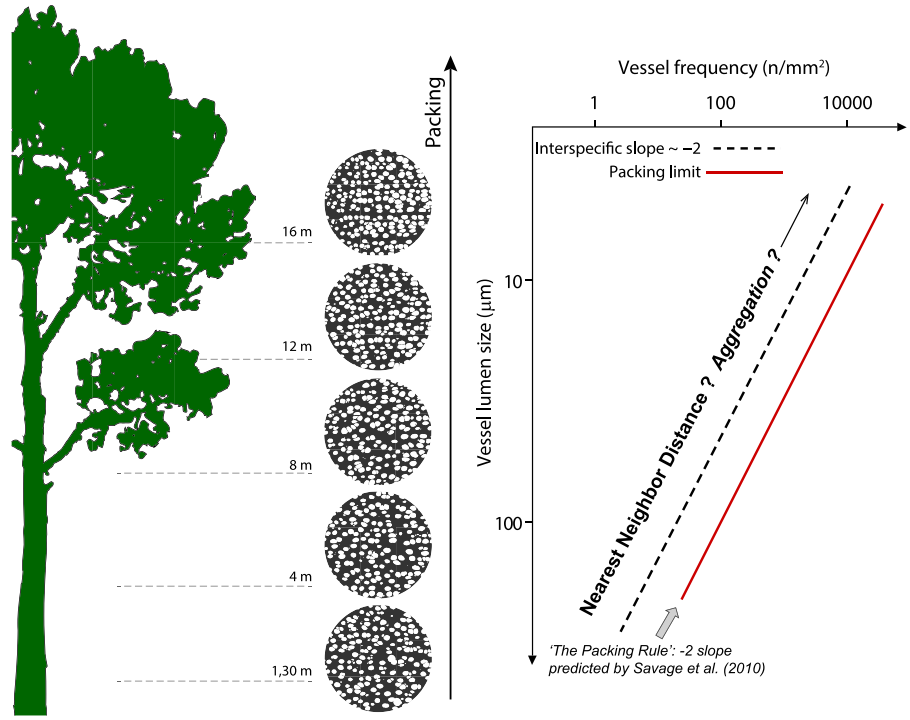

Figure 1. Simplified representation of *Fagus sylvatica* xylem slides from the collected stem cross-sections at different heights on the left. On the right, the typical theoretical basipetal trade-off between vessel lumen size and vessel frequency following the "packing rule", inspired by Sperry *et al.* (2008). The relationship across functional groups varies approximately inversely with the square of the conduit radius where the dashed line represents the interspecific exponent from the literature. The full line represents the modelled packing exponent by Savage *et al.* (2010).

common diffuse-porous temperate species, growing in two contrasting bioclimatic sites along the Italian Apennines. We expected a distinct spatial pattern of vessels according to ontogenetic factors, where vessel proximity and aggregation would increase with tree height and age.

MATERIALS AND METHODS

Study sites and radial strip sampling

Eight dominant *F. sylvatica* L. adult trees were felled from two study sites and their heights were measured. The first site was an even-aged *F. sylvatica* stand in the Abetone forest (Northern Apennines; 44.10°N, 10.70°E; 1300 m a.s.l.) characterized by a perhumid climate with 2449 mm of annual precipitation and mean annual temperature of 11.6°C. The second site was chosen in Serra San Bruno (Southern Apennines; 38.56°N, 16.29°E; 1050 m a.s.l.), where the climate is typically Mediterranean with hot dry summers and predominantly winter rainfall. The annual precipitation is 1789 mm and the mean annual temperature is 11.5°C. For each tree, we took five transversal stem discs at five different heights along the main stem (1.30 m, 4.00 m, 8.00 m, 12.00 m, and 16.00 m above the ground) (Table 1). We recognize that the sampling strategy (sectioning from bottom to top) might partially influence the result we obtained since at the very distal branch segments the conduit tapering is strongest and the packing rule should apply most strongly. The width of tree-rings was first measured to the nearest 0.01 mm using a tree-ring measuring system (LINTAB 6 coupled with TSAP-Win Scientific software, Rinntech, Heidelberg, Germany) and then visually cross-dated. Cross-dating was checked statistically using COFECHA software (Holmes & Fritts 1986). Further details of stand characteristics, sampling strategy, and cross-dating are described in Gentilesca *et al.* (2018). The retrospective reconstruction of annually-resolved height growth rates, as well as the distance from the apex to the stem base (D_{apex}), was generated by stem analysis using ring-width data sampled from successive sections along the stems with the "*IncrementR*" package (Kašpar *et al.* 2019) in R v.3.6.0 (R development Core Team 2019).

Woody sample preparation and image processing

For each collected disc, one radial strip (1 cm wide) running from bark to pith was selected to analyse the entire radial growth. Samples were first checked to exclude reaction wood, eccentricities, or wounding and then radial woody samples were split into 3–4 cm long pieces for processing. Next, anatomical cross-sections (15–20 µm thickness) were cut with a sliding

Table 1.
Summary of sampled tree features measured in the two study sites.

	ID	Age	DBH (cm)	*H* (m)	TRW (mm)	C. int.
Site1	1	82	28.5	25	1.17 (0.55)	2002–2015
	2	69	29	24.6	1.94 (0.18)	1999–2015
	3	75	27.5	22.3	1.24 (0.27)	2001–2015
Site2	4	79	37.8	24.5	2.54 (0.74)	1975–2014
	5	84	49.5	25.8	2.82 (0.64)	1986–2014
	6	60	32	26.6	1.95 (0.63)	1987–2014
	7	95	35.5	27	2.00 (0.58)	1978–2014
	8	93	44.5	27.2	2.22 (0.91)	1958–2014

Site 1, Abetone; Site 2, Serra San Bruno. DBH (cm), diameter at breast height; *H* (m), tree height; TRW (mm), mean tree-ring width at breast height; C. int., common interval time span. Standard deviation of the mean is shown in parentheses.

microtome (Microm HM 400, Thermo Sci., Walldorf, Germany), stained with Safranin (1%) and Astra Blue (2%), and fixed on permanent slides with Eukitt balsam (Kindler, Freiburg, Germany). Digital images were captured at 5× magnification (1 pixel = 1.22 μm) with an integrated digital camera (DCM300, ScopeTek) installed on a light microscope (Zeiss Axiophot, Carl Zeiss Microscopy, Jena, Germany). Overlapping images of the whole micro-section were stitched with Image Composite Editor software (ICE 2.0.3, Microsoft, Redmond, WA, USA). A semi-automated image processing using ImageJ software (National Institutes of Health, Bethesda, MD, USA) was employed to determine for each tree-ring the x and y coordinates of the centers of each vessel, as well as their respective lumen areas using 200 μm^2 as the minimum measurement threshold (see Fig. A1 in the Appendix). Careful visual inspection was necessary to exclude non-vascular elements or include vessels that had not been selected. Then, for each tree-ring, we calculated the average vessel area (A_{av}) and vessel density (D_v) as the number of vessels per unit of surface area.

Statistical analyses

Point pattern analysis (PPA) was used to (i) detect whether the spatial patterns of the xylem conduits significantly departed from randomness and (ii) interpret patterns of vessel distribution in xylem cross-sections. Useful aspects of this general spatial stochastic process were characterized in terms of first-order and second-order properties. Briefly, the first-order statistics were used to describe the large-scale variation in the local intensity of vessels in a study region, whereas second-order statistics described the interaction (clustering) among values of the process over space. To this end, a hyperframe that included a tree-ringwise spatial dataset (containing marked values of the vessel area attached to the points) for the common interval (Table 1) was built to perform all statistical analyses with the "*spatstat*" (Baddeley 2015) package in R v.3.6.0 (R development Core Team 2019).

Modeling vessel occurrence process — first-order spatial pattern

As conduit density can vary for different portions of stems, we first investigated the spatial processes that may govern the distribution of xylem conduits as a function of the distance of sampled stem cross-section from the stem apex (D_{apex}). The relationship between the xylem conduit pattern intensity and the aforementioned spatial covariates was modelled following a Poisson point process model. A Poisson point process is completely described in terms of intensity $\lambda(u)$ of the process, which is the expected probability of finding a certain number of conduits per unit area at the point u (Diggle & Cox 1983). This is defined as the mathematical limit:

$$\lambda(u) = \lim_{du \leftarrow 0} \left\{ \frac{E(Y(du))}{du} \right\}$$

where du is a small region around the point u, $E(\cdot)$ is the expectation operator, and $Y(du)$ refers to the number of events in this small region. That is, more vessels are expected in locations where the intensity function is high, and fewer vessels are expected in locations where the intensity function is low. In its classical form, points take a random spatial distribution and are independent of one another (Cressie & Wikle 2015). When points are stationary their density is proportional to the area and they display an homogeneous pattern, and the probability intensity function takes the form:

$$\lambda(u) = e^{\beta_0}.$$

Nonstationary Poisson models are documented when the intensity is conditioned by covariates, thereby creating inhomogeneity and is fitted via a log-linear function of the covariates (Baddeley 2015):

$$\lambda(u) = e^{\beta_0+\beta_1 Z(u)+\beta_2 S(u)}$$

with intensity in the form $\lambda(u)$ at location u, where β_0, β_1 and β_2 are coefficients to be estimated, and $Z(u)$ and $S(u)$ are the values of the covariates at location u.

To evaluate the intensity of conduits, while still accounting for unknown random variability, we used a mixed-effects point process model for multiple point patterns (MPPM). MPPMs are similar in structure and output to the generalized linear models. The key difference is that the response variable is a series of point patterns for which the intensity is a function of a covariate (Baddeley 2015), namely D_{apex} (fixed effect). Random effects were included to account for unknown variability amongst trees.

Comparisons between spatially homogeneous and heterogeneous Poisson models were performed using the likelihood ratio test (LRT) of the null hypothesis of a homogeneous Poisson process (CSR) against the alternative of an inhomogeneous Poisson process with an intensity that is a log-linear function of the covariates. The model that minimized the Akaike Information Criterion (AIC) value was chosen as the best fit. Model validation was performed using an analysis of deviance (ANOVA) for MPPM and a residual K-function (goodness of fit test) to access model accuracy according to Baddeley (2015).

Characterizing spatial point patterns — second-order spatial patterns

Because neither the intensity nor the spatial density provides any information on the interaction between two arbitrary xylem conduits, we performed the second-order spatial statistics, which reflect any tendency of the events to appear clustered, independent, or regularly spaced (Diggle 2013). Thus, the spatial arrangement of vessels at each position along the stem was assessed by calculating the average nearest neighbour distance (NN_d) with the '*nndist*' function, which computed the Euclidean distance from each vessel in a point pattern to its nearest neighbour (the nearest other point in the pattern). Low values of NN_d indicated an increase in vessel connectivity, whereas higher values denoted greater isolation of vessels with respect to neighbouring vessels. Then, we inspected the pattern of NN_d with the cambial age, the tree-ring width, and the height of the cross-section (1.30, 4.00, 8.00, 12.00 and 16.00 m) by fitting a linear mixed-effects model (LMM) using the library "*nlme*" available in the R statistical suite, where the tree ID was included as a random component. The maximum-likelihood method (ML) and restricted maximum-likelihood method (REML) were respectively applied to estimate fixed-effects terms and optimal random structure. Residual error variance and correlation structure were explicitly integrated into the models to include measurement heterogeneity and independence.

Initially, we entered all variables (D_{apex}, cambial age (CA) and tree-ring width (TRW)) with their interactions as fixed effects into the model (full model). The model with the smallest AIC value was chosen as the best fit using the "*MuMIn*" dredge function (Barton 2020) when the ΔAICc values (Akaike Information Criterion corrected for sample size) were >10. We test the significance of fixed effects and their interactions with LR tests using the Anova function. Marginal and conditional R^2 scores (Nakagawa & Schielzeth 2013) were calculated to examine the variation explained by models using the "*r.squaredGLMM*" function in the "*MuMIn*" package.

The nonparametric Ripley's K-function (Haase 1995) was calculated to characterize spatial patterns (clustering or regularity) of vessel elements within tree-rings. The concept behind Ripley's K-function is rather simple; it is the average number of events (xylem vessels) located within a predefined radius "r" of any typical event, normalized for the event intensity (density) over the same field of view. Intuitively, the distribution of estimated K events (described as $K(r) = \lambda - 1E$, equals the expected (E) number of vessels within the distance r of the typical random vessel x) is usually compared to the true K value from the Complete Spatial Randomness model (CSR, null model, which is $K(r) = \pi r^2$), otherwise known as the "homogeneous Poisson process." Deviations between the empirical and theoretical K values may suggest spatial clustering or spatial regularity: for a regular pattern $K(r) < \pi r^2$, whereas under clustering $K(r) > \pi r^2$ (Bailey & Gatrell 1995). Edge effects (a circle centered at a point too close to the boundary to be evaluated without a bias) was mitigated by Ripley's isotropic correction method (Ripley 1988; Diggle 2013).

The L-function ($L(r)$) was used for simpler interpretation by normalizing the K-function to obtain a benchmark of zero (Diggle and Cox 1983):

$$L(r) = \sqrt{K(d)/\pi} - r.$$

The $L(r)$ value indicates the degree of clumping or overdispersion. Values of $L(r) > 0$ indicates a clumped pattern, a greater number of vessels than would be expected if the individuals were randomly distributed, and $L(r) < 0$ indicates an overdispersed pattern, few vessels within a scale of r than would be expected if the vessels were randomly distributed (L values >0 indicate spatial attraction of events (clustering) and negative values indicate spatial repulsion (dispersion). The value of $L(r)$

also explains the degree of clumping and/or overdispersion. The value of $L(r)$ plus the value of r is the radius of the circle in which the same number of vessels would be observed in case of a completely random distribution.

RESULTS

Overall A_{av} showed a hump-shaped increasing pattern towards the tree base, whereas D_v decreased. The average vessel area showed a 2-fold reduction (0.0022 to 0.0010 mm², average values) from stem base to top (Fig. 2). However, for vessel density, there was a moderate increase in vessel number along the xylem pathway. Both vessel lumen diameter and frequency showed a unimodal distribution in the studied *F. sylvatica* trees, consistent with diffuse-porous tree species, although vessel lumen density distribution was slightly right-skewed, indicating that approx. 115 vessels/mm² were highly frequent.

Poisson point process model with a covariate effect

Table 2 shows the estimated intensity according to the parametric model. The null model (homogeneous Poisson) fitted to the data had a constant intensity, valued $e_{4.78}$ = 120.03 mm² over the entire region. This constant intensity could be interpreted as an average of approximately 120 vessel occurrences for every 1 mm² in all tree-rings. The estimated probability of vessels decreased by $e^{-0.0002}$ = 0.99 for every meter of distance to the tree apex.

Characterizing spatial point patterns — second-order spatial patterns

Increased nearest neighbour distances (NN_d) among xylem vessels was mainly the result of an increase in vessel frequency but not necessarily a decrease in their average lumen size (Fig. 3b). This finding was supported by a strong negative relationship between NN_d and D_v and by a weaker correlation with A_{av}. The effect sizes for the LMM used to analyse the combined

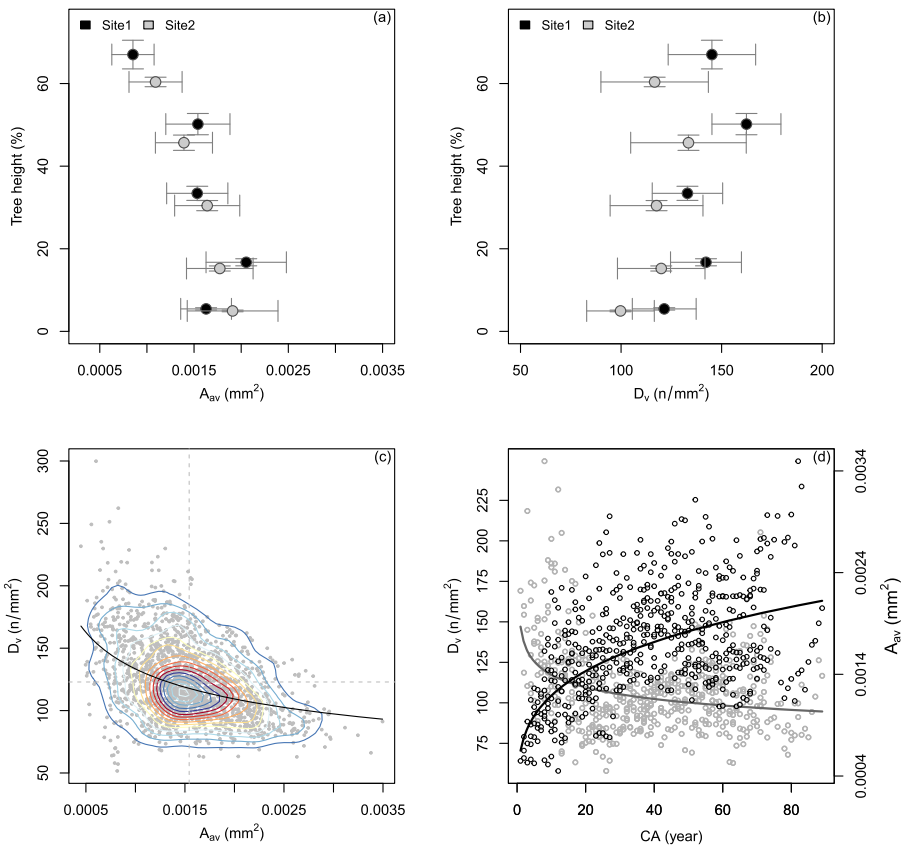

Figure 2. The pattern of average vessel size (A_{av}) and vessel density (D_v) for the common interval along with stem cross-sectional heights (*a* and *b*, respectively). Each data point represents the mean value obtained from the five different sampling heights, whereas whiskers are standard errors. Filled and empty circles represent Site 1 and Site 2, respectively. The inverse relationship between A_{av} and D_v along with the density distribution of points (*c*) with contour lines; interpolation line is an exponential regression (D)v = 18.36·$A_{av}^{-0.28}$; $F_{(1,1721)}$ = 338.4, p < 0.001, R^2 = 0.17). The pattern of A_{av} (black circles, A_{av} = 0.0006·$CA^{0.26}$; $F_{(1,519)}$ = 287.2, p < 0.001, R^2 = 0.35) and D_v (grey circles, D_v = 147.01·$CA^{-0.09}$; $F_{(1,519)}$ = 72.3, p < 0.001, R^2 = 0.12) with cambial age (CA) (*d*) where interpolation lines are exponential regressions.

Table 2.
Summary of statistics for the fitted Poisson models.

	Est.	Std. Error	*t* value	Pr(> |*t*|)
Intercept	4.7877	3.58E-03	1335.569	***
D_{apex}	−0.0002	2.93E-06	−58.697	***

Est, estimates; Std. Error, standard error; D_{apex}, distance to the stem apex.
*** Statistically significant at $P < 0.001$.

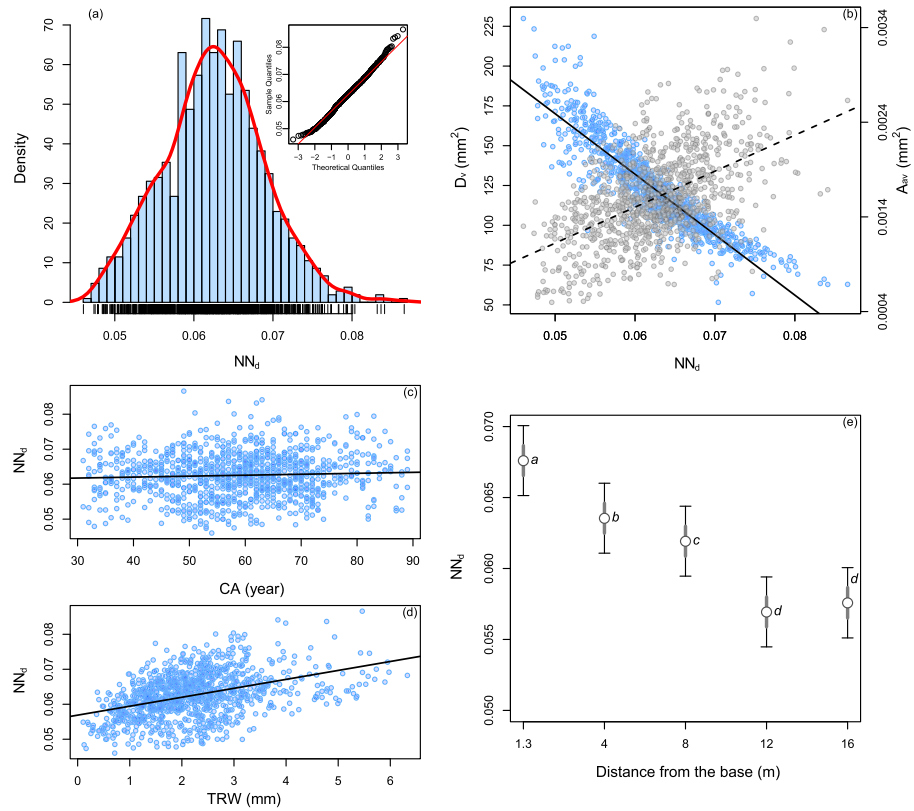

Figure 3. Nearest neighbour distance (NN_d) density distribution of xylem vessels (*a*). Linear relationships between NN_d and average vessel size (dashed line, A_{av} = -0.0007 + 0.038·NN_d, $F_{(1,1730)}$ = 981.5, *p*-value < 0.001, R^2 = 0.36) and vessel density (full line, D_v = 360–3798.4 · NN_d, $F_{(1,1730)}$ = 9046.1, *p*-value < 0.001, R^2 = 0.83) (*b*). Effect sizes of the fitted linear models showing the linear relationship between NN_d of xylem vessels and cambial age (slope $\beta_{std.}$ = 0.19) (*c*) and the tree-ring width (slope $\beta_{std.}$ = 0.46) (*d*), and the variability of nearest neighbour distance of xylem vessels among the five different sampling points along the stem flow path (1.30 m, 4.00 m, 8.00 m, 12.00 m, and 16.00 m) (*e*). Differences among the linear fit values were tested using an analysis of co-variance and the post hoc Tukey's honestly significant difference test (HSD) with the "lsmeans" package (Lenth 2016). Points represent the estimated marginal means (EMMs) of linear trends (β), the tick lines are 95% confidence intervals of the linear trend estimates, and the arrows are for comparisons among them. If an arrow from one mean overlaps an arrow from another, the difference is not significant. Pairwise significant ($p < 0.05$) differences among the linear fits were tested with the post hoc Tukey's HSD. Different letters near arrows indicate significant differences among estimated linear trends.

effect of D_{apex}, TRW, and CA on the NN_d of vessels is shown in Fig. 3c–e, whereas the model structures, covariates with model coefficients, standard errors, and significance levels are summarized in Table A1 in the Appendix. In detail, the proportion of variance explained by the fixed factor(s) alone in the model was 51%. A rather large proportion of total variance was explained by trees within sites, as shown by the intraclass correlation coefficients (ICC = 0.43). The fitted model indicated a significant negative effect of distance from the tree base, a positive effect of TWR, and a positive weak effect of CA on NN_d, suggesting that xylem vessels were closer to each other near the apex and became progressively more distant toward the stem base. The spatial pattern of xylem vessels in our samples appeared to violate the assumption of complete random spatial distribution (Fig. 4, Fig. A3 in the Appendix). Particularly, the *L*-function ($L(r)$, Besag's transformation of Ripley's *K*-function) showed

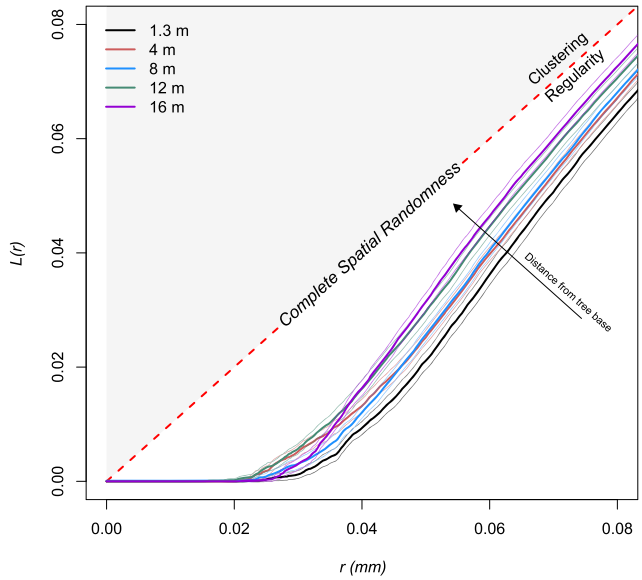

Figure 4. L-function (mean number of vessels within radius r from any vessel) for the observed point pattern (isotropic-corrected estimate of $L(r)$) plus high and low confidence intervals (grey lines), theoretical value under complete spatial randomness (dashed line). The *x*-axis shows the distance argument r in mm.

regularity occurred at all scales of analysis, vessel spatial arrangement followed a uniform distribution at different distances from the tree base. Worth emphasising is the decreasing offset of the estimate of $L(r)$ from the CRS at increasing distance from the stem base.

DISCUSSION

The typical vessel distribution pattern of *F. sylvatica* consists of xylem vessels with more or less equal diameter uniformly distributed throughout the annual ring, leaving early- and late-wood fairly indistinct. However, such a pattern does not remain fixed but is subject to modification attributed to a suite of adaptations induced by physiological constraints driven by both ontogenetic development and environmental characteristics (Anfodillo *et al.* 2006; Schuldt *et al.* 2016).

Progressive increase in intensity (lambda) from the apex to the base in our samples is completely in agreement with the "packing rule" theory and supported by former reports showing an increasing number of vessels concomitant with a decreasing average lumen area along the stem pathway, which might be intuitively obvious because fewer larger vessels can fit into a given space than small ones (Savage *et al.* 2010, and references therein). Basipetal vessel widening ensures that most of the path length resistance lies within a short distance from the apex, thus promoting the maintenance of total xylem hydraulic resistance irrespective of absolute tree height (West *et al.* 1999; Anfodillo *et al.* 2006).

Although from the anatomical and structural point of view, the intensity (lambda) might express an increasing probability of vessels being in contact in a given sample at increasing tree height, it does not take into account the spatial distance between xylem vessels in our samples. In this regard, the distance between adjacent vessels (NN_d) appears as a direct consequence of lambda variation, (it proportionally increased with increasing tree height) such that NN_d was smallest at the tree apex and progressively increased towards the stem base. Our observation that axial variation in NN_d is similar to that found by other studies (Lechthaler *et al.* 2019) again highlights the strong role played by the path length, and thus by the plant size, in shaping the hydraulic architecture of the xylem, although our findings suggested that tree identity and/or the sampling strategy (sectioning from bottom to top) should not be neglected (see intraclass correlation coefficient in Table A1 in the Appendix). Quite surprisingly, our results underscore that even if a positive correlation between vessel density and the average lumen of vessels is to be expected, they were not similarly related to the NN_d suggesting that vessel density and not their lumen area had the most to do with the probability of physical contact or proximity to the nearest neighbours as observed by Jansen *et al.* (2011) and Schuldt *et al.* (2016). The spatial arrangement of vessels has often been proposed to be important for their reciprocal interconnections, with potentially implications for the safety-efficiency trade-off of the water transport system. The smaller intervessel distance (NN_d) close to the apex supports the hypothesis that pathway redundancy (expressed by percentage of wall surface in common; Tyree *et al.* 1994) allows water to more easily bypass embolized vessels (Loepfe *et al.* 2007; Trifilò *et al.* 2014). Many influences of vessel connectivity, also referred to as vessel grouping in a transverse section

(Carlquist 1984), on plant performance have so far been postulated only theoretically. Several models have demonstrated that redundancy might be an advantageous strategy to increase hydraulic conductivity and water transport efficiency (Martínez-Vilalta *et al.* 2012), which in turn may stimulate growth (Nielsen *et al.* 2017) because water can bypass cavitated vessels (Hölttä *et al.* 2006). Another benefit of vessel redundancy is related to the observed increase in permeability of intervessel pit membranes upon changes in the ionic concentration of the xylem sap, which can occur during water limitation ("ionic effect" of Jansen *et al.* 2011). On the other hand, increased vessel redundancy can also bring disadvantages mostly under dry conditions because vessels in a dense network have more contact surface, which enhances the risk of drought-induced cavitation caused by air seeding under extreme xylem tension through the intervessel pits, also known as the "air-seeding" hypothesis (Loepfe *et al.* 2007). Our results also indicated that the tree-ring width could partially interfere with the axial pattern of NN_d outlined above since variability in tree-ring width, wider/narrower rings (also arising from an imperfect eccentricity of the stem or wounding, Arbellay *et al.* 2012; Kašpar *et al.* 2019) might show a certain variability in xylem anatomical traits as well such as lower/higher number of vessels per unit of tree-ring surface of *F. sylvatica* mainly because of the higher proportion of latewood (Eilmann *et al.* 2014; Diaconu *et al.* 2016). In such cases, the diffuse-porous wood structure can tend to a semi-ring porous structure regarding the tree ring width (Schweingruber, 2007).

However, as previously explained, NN_d quantifies only one aspect of the spatial patterns, that related to physical closeness to the nearest neighbour, and hence it may be regarded as being closer to the definition of the traditional anatomical grouping indices (Carlquist 2001), with less emphasis on physical contact among conduits. In this regard, the Ripley's *K*-function may be considered the novel "gold standard" in spatial point analysis, mostly in classifying the degree of vessel arrangement in the growth rings compared to the well-established grouping indices, such as the vessel grouping index (VG) and Clark & Evans uniformity index (Clark & Evans 1954; Scholz *et al.* 2013), which are averaged values with limited functional information that do not quantify clustering at different scales.

Theoretically, given the range of diameters and density of vessels in a given species and in a given annual growth ring, a certain number of vessels will be in contact if their distribution is determined as being random or clustered. However, a major finding of this study is that while xylem vessel distance decreases along the stem because of packing (Sperry *et al.* 2008; Savage *et al.* 2010), the hypothesis of clustering of the vessel was not supported by our results. Rather, point pattern profiles clearly highlighted a lack of aggregation of vessels in the face of a regular spatial distribution of vessels through the growth ring along the entire pathway. Thus, when increasing the frequency of vessels at decreasing distance to the tree apex in diffuse-porous wood, clustering will not occur merely because of packing. We argue that properties related to vessel clustering more likely involve a functional significance, mostly related to the hydraulic adjustments in response to environmental constraints over a plant's lifetimes, rather than a simple mechanistic explanation. The acclimatization of structural characteristics of xylem and the plasticity of the whole-plant morphology in response to environmental constraints could have a major role in determining xylem conduit aggregation. In part, this could be explained by the fact that both vessel diameter and frequency, as well as their spatial arrangement, are influenced not only by ontogenesis (tree size) but certainly also by other site-specific biotic and abiotic factors, such as soil properties, and in particular, nutrient availability (Borghetti *et al.* 2017), and climatic conditions (Fonti *et al.* 2010; Rita *et al.* 2015) coupled with habitat dryness (Robert *et al.* 2009; Jansen *et al.* 2011; Castagneri *et al.* 2019). Recent findings indeed showed consistent relationships between VG and strong reductions in water supply across several regions (von Arx *et al.* 2013; Nielsen *et al.* 2017). Coherently, Schuldt *et al.* (2016) also provided additional support for the assumption that *F. sylvatica* is highly plastic with respect to embolism resistance under water-limited environments increasing the safety of the conductive hydraulic system by pathway redundancy.

CONCLUSIONS

By analysing xylem vessel features in a long-term anatomical time series of *F. sylvatica* L. taken at different stem heights we challenged the hypothesis of an ontogenetic effect on the vessels' spatial distribution inside tree-rings. In particular, we evaluated whether the Sperry's "packing rule" would affect either xylem spatial intensity, proximity, or conduit aggregation. Our results indicated that the probability of finding a greater number of vessels within the annual tree-ring increases with the distance from the stem base, and the distance between neighbouring vessels is reduced. This is completely in agreement with the "packing rule" theory, which predicts vessels packing in gradually smaller areas, where the frequency of xylem conduits varies approximately inversely with the square of the conduit radius. We showed that the distance among neighbouring vessels is much more dependent on the vessel frequency than their lumen area, suggesting an increased probability of vessels to touch along the tree path. Although there is an increase in the intensity and proximity among vessels, we demonstrated that no patterns of aggregation between vessels existed. Rather, point pattern profiles clearly highlighted a lack of aggregation of vessels in the face of a regular spatial distribution of vessels in the growth rings along with stems. Thus, increasing the frequency of vessels at decreasing distance to the tree apex in diffuse-porous wood, the grouping will not occur merely

because of packing. We argued that although the importance of vessel clustering has been recognized by many authors as a valid compromise to maximize hydraulic efficiency within the xylem network, our results sustain the hypothesis that the clustering of vessels may be affected more by the environmental variability (climate) rather than by ontogenetic constraints.

ACKNOWLEDGEMENTS

The research was supported by the MIUR-PRIN Grant No. 2012E3F3LK 'Global change effects on the productivity and radiative forcing of Italian forests: a novel retrospective, experimental and prognostic analysis'. AR and OP was supported and co-founded by the project "Advanced EO Technologies for studying Climate Change impacts on the environment — OT4CLIMA" which was funded by the Italian Ministry of Education, University and Research (D.D. 2261 del 6.9.2018, PON R&I 2014–2020 e FSC) and OP by the PhD program in 'Agricultural, Forest and Food Sciences' at the University of Basilicata, Potenza — Italy. We thank A. Lapolla (University of Basilicata, Potenza — Italy) for field support in trees sampling. We are also grateful to two anonymous referees for their helpful and constructive comments that greatly improved the article.

REFERENCES

Anderegg WRL, Konings AG, Trugman AT, Yu K, Bowling DR, Gabbitas R, Karp DS, Pacala S, Sperry JS, Sulman BN, Zenes N. 2018. Hydraulic diversity of forests regulates ecosystem resilience during drought. Nature 561: 538–541. DOI: 10.1038/s41586-018-0539-7.

André JP, Catesson AM, Liberman M. 1999. Characters and origin of vessels with heterogenous structure in leaf and flower abscission zones. Can. J. Bot. 77: 253–261.

Anfodillo T, Carraro V, Carrer M, Fior C, Rossi S. 2006. Convergent tapering of xylem conduits in different woody species. New Phytol. 169: 279–290. DOI: 10.1111/j.1469-8137.2005.01587.x.

Arbellay E, Fonti P, Stoffel M. 2012. Duration and extension of anatomical changes in wood structure after cambial injury. J. Exp. Bot. 63: 3271–3277. DOI: 10.1093/jxb/ers050.

Baas P, Carlquist S. 1985. A comparison of the ecological wood anatomy of the floras of southern California and Israel. IAWA J. 6: 349–353. DOI: 10.1163/22941932-90000961.

Baddeley A. 2015. Spatial point patterns: methodology and applications with R. Chapman and Hall/CRC Press, Boca Raton, USA.

Bailey TC, Gatrell AC. 1995. Interactive spatial data analysis. Prentice-Hall, NJ, USA.

Barton K. 2020. MuMIn: Multi-Model Inference. R package version 1.43.17. https://CRAN.R-project.org/package=MuMIn.

Borghetti M, Gentilesca T, Leonardi S, van Noije T, Rita A. 2017. Long-term temporal relationships between environmental conditions and xylem functional traits: a meta-analysis across a range of woody species along climatic and nitrogen deposition gradients. Tree Physiol. 37: 4–17. DOI: 10.1093/treephys/tpw087.

Carlquist S. 1984. Vessel grouping in dicotyledon wood. Aliso 10: 505–525. DOI: 10.5642/aliso.19841004.03.

Carlquist S. 2001. Comparative wood anatomy. Springer Verlag, Berlin, Germany.

Carlquist S. 2009. Non-random vessel distribution in woods: patterns, modes, diversity, correlations. Aliso 27: 39–58. DOI: 10.5642/aliso.20092701.04.

Castagneri D, Carrer M, Regev L, Boaretto E. 2019. Precipitation variability differently affects radial growth, xylem traits and ring porosity of three Mediterranean oak species at xeric and mesic sites. The Science of the Total Environment 699: 134285. DOI: 10.1016/j.scitotenv.2019.134285.

Clark PJ, Evans FC. 1954. Distance to nearest neighbor as a measure of spatial relationships in populations. Ecology 35: 445–453. DOI: 10.2307/1931034.

Cressie N, Wikle CK. 2015. Statistics for spatio-temporal data. John Wiley & Sons, NJ, USA.

Diaconu D, Stangler DF, Kahle HP, Spiecker H. 2016. Vessel plasticity of European beech in response to thinning and aspect. Tree Physiol. 36(10): 1260–1271. DOI: 10.1093/treephys/tpw053.

Diggle PJ. 2013. Statistical analysis of spatial and spatio-temporal point patterns, 3rd Edn. CRC Press, Boca Raton, USA.

Diggle PJ, Cox TF. 1983. Some distance-based tests of independence for sparsely-sampled multivariate spatial point patterns. International Statistical Review/Revue Internationale de Statistique 51: 11.

Eilmann B, Sterck F, Wegner L, de Vries SMG, von Arx G, Mohren GMJ, den Ouden J, Sass-Klaassen U. 2014. Wood structural differences between northern and southern beech provenances growing at a moderate site. Tree Physiol. 34(8): 882–893. DOI: 10.1093/treephys/tpu069.

Fonti P, Von Arx G, García-González I, Eilmann B, Sass-Klaassen U, Gartner H, Eckstein D. 2010. Studying global change through investigation of the plastic responses of xylem anatomy in tree rings. New Phytol. 185: 42–53. DOI: 10.1111/j.14698137.2009.03030.x.

Gentilesca T, Rita A, Brunetti M, Giammarchi F, Leonardi S, Magnani F, van Noije T, Tonon G, Borghetti M. 2018. Nitrogen deposition outweighs climatic variability in driving annual growth rate of canopy beech trees: evidence from long-term growth reconstruction across a geographic gradient. Global Change Biol. 24: 2898–2912. DOI: 10.1111/gcb.14142.

González-Cásares M, Julio Camarero J, Colangelo M, Rita A, Pompa-García M. 2019. High responsiveness of wood anatomy to water availability and drought near the equatorial rear edge of Douglas-fir. Can. J. Forest Res. 49: 1114–1123. DOI: 10.1139/cjfr-2019-0120.

Haase P. 1995. Spatial pattern analysis in ecology based on Ripley's K-function: introduction and methods of edge correction. J. Veg. Sci. 6: 575–582. DOI: 10.2307/3236356.

Hacke UG, Sperry JS. 2001. Functional and ecological xylem anatomy. Perspectives in Plant Ecology, Evolution and Systematics 4: 97–115. DOI: 10.1078/1433-8319-00017.

Holmes RL, Fritts HC. 1986. Tree-ring chronologies of western North America: California, eastern Oregon and northern great basin with procedures used in the chronology development work including user's manuals for computer programs COFECHA and ARSTAN. https://repository.arizona.edu/handle/10150/304672.

Hölttä T, Vesala T, Perämäki M, Nikinmaa E. 2006. Refilling of embolised conduits as a consequence of "Münch water" circulation. Funct. Plant Biol. 33: 949. DOI: 10.1071/FP06108.

IAWA Committee. 1989. IAWA list of microscopic features for hardwood identification. IAWA Bull. 10: 219–332.

Jansen S, Gortan E, Lens F, Lo Gullo MA, Salleo S, Scholz A, Stein A, Trifilò P, Nardini A. 2011. Do quantitative vessel and pit characters account for ion-mediated changes in the hydraulic conductance of angiosperm xylem? New Phytol. 189: 218–228. DOI: 10.1111/j.1469-8137.2010.03448.x.

Kašpar J, Tumajer J, Treml V. 2019. IncrementR: analysing height growth of trees and shrubs in R. Dendrochronologia 53: 48–54. DOI: 10.1016/j.dendro.2018.11.001.

Lechthaler S, Turnbull TL, Gelmini Y, Pirotti F, Anfodillo T, Adams MA, Petit G. 2019. A standardization method to disentangle environmental information from axial trends of xylem anatomical traits. Tree Physiol. 39: 495–502. DOI: 10.1093/treephys/tpz068/5519844.

Lens F, Sperry JS, Christman MA, Choat B, Rabaey D, Jansen S. 2011. Testing hypotheses that link wood anatomy to cavitation resistance and hydraulic conductivity in the genus *Acer*. New Phytol. 190: 709–723. DOI: 10.1111/j.1469-8137.2010.03518.x.

Lenth RV. 2016. Least-squares means: the R package lsmeans. J. Stat. Softw.: 69. DOI: 10.18637/jss.v069.i01.

Loepfe L, Martinez-Vilalta J, Piñol J, Mencuccini M. 2007. The relevance of xylem network structure for plant hydraulic efficiency and safety. J. Theor. Biol. 247: 788–803. DOI: 10.1016/j.jtbi.2007.03.036.

Martínez-Vilalta J, Mencuccini M, Alvarez X, Camacho J, Loepfe L, Piñol J. 2012. Spatial distribution and packing of xylem conduits. Am. J. Bot. 99: 1189–1196. DOI: 10.3732/ajb.1100384.

McCulloh K, Sperry JS, Lachenbruch B, Meinzer FC, Reich PB, Voelker S. 2010. Moving water well: comparing hydraulic efficiency in twigs and trunks of coniferous, ring-porous, and diffuse-porous saplings from temperate and tropical forests. New Phytol. 186: 439–450. DOI: 10.1111/j.1469-8137.2010.03181.x.

Mencuccini M, Manzoni S, Christoffersen B. 2019. Modelling water fluxes in plants: from tissues to biosphere. New Phytol. 222: 1207–1222. DOI: 10.1111/nph.15681.

Mencuccini M, Martinez-Vilalta J, Piñol J, Loepfe L, Burnat M, Alvarez X, Camacho J, Gil D. 2010. A quantitative and statistically robust method for the determination of xylem conduit spatial distribution. Am. J. Botany 97: 1247–1259. DOI: 10.3732/ajb.0900289.

Nakagawa S, Schielzeth H. 2013. A general and simple method for obtaining R2 from generalized linear mixed-effects models. Methods Ecol. Evol. 4: 133–142. DOI: 10.1111/j.2041-210x.2012.00261.x.

Nardini A, Dimasi F, Klepsch M, Jansen S. 2012. Ion-mediated enhancement of xylem hydraulic conductivity in four *Acer* species: relationships with ecological and anatomical features. Tree Physiol. 32: 1434–1441. DOI: 10.1093/treephys/tps107.

Nielsen SS, von Arx G, Damgaard CF, Abermann J, Buchwal A, Büntgen U, Treier UA, Barfod AS, Normand S. 2017. Xylem anatomical trait variability provides insight on the climate-growth relationship of *Betula nana* in western Greenland. Arct. Antarct. Alp. Res. 49: 359–371. DOI: 10.1657/AAAR0016-041.

Page GFM, Liu J, Grierson PF. 2011. Three-dimensional xylem networks and phyllode properties of co-occurring *Acacia*. Plant Cell Environ. 34: 2149–2158. DOI: 10.1111/j.1365-3040.2011.02411.x.

Petit G, Pfautsch S, Anfodillo T, Adams MA. 2010. The challenge of tree height in *Eucalyptus regnans*: when xylem tapering overcomes hydraulic resistance. New Phytol. 187: 1146–1153. DOI: 10.1111/j.1469-8137.2010.03304.x.

Ripley BD. 1988. Statistical inference for spatial processes. Cambridge University Press, UK.

Rita A, Cherubini P, Leonardi S, Todaro L, Borghetti M. 2015. Functional adjustments of xylem anatomy to climatic variability: insights from long-term *Ilex aquifolium* tree-ring series. Tree Physiol. 35: 817–828. DOI: 10.1093/treephys/tpv055.

Robert EMR, Koedam N, Beeckman H, Schmitz N. 2009. A safe hydraulic architecture as wood anatomical explanation for the difference in distribution of the mangroves *Avicennia* and *Rhizophora*. Funct. Ecol. 23: 649–657. DOI: 10.1111/j.1365-2435.2009.01551.x.

Ryan MG, Phillips N, Bond BJ. 2006. The hydraulic limitation hypothesis revisited. Plant Cell Environ. 29: 367–381. DOI: 10.1111/j.1365-3040.2005.01478.x.

Savage JA, Clearwater MJ, Haines DF, Tamir K, Mencuccini M, Sevanto S, Turgeon R, Zhang C. 2016. Allocation, stress tolerance and carbon transport in plants: how does phloem physiology affect plant ecology? Plant Cell Environ. 39: 709–725. DOI: 10.1111/pce.12602.

Savage VM, Bentley LP, Enquist BJ, Sperry JS, Smith DD, Reich PB, von Allmen EI. 2010. Hydraulic trade-offs and space-filling enable better predictions of vascular structure and function in plants. PNAS 107: 22722–22727. DOI: 10.1073/pnas.1012194108.

Scholz A, Klepsch M, Karimi Z, Jansen S. 2013. How to quantify conduits in wood? Front. Plant Sci. 4: 56. DOI: 10.3389/fpls.2013.00056.

Schuldt B, Knutzen F, Delzon S, Jansen S, Müller-Haubold H, Burlett R, Clough Y, Leuschner C. 2016. How adaptable is the hydraulic system of European beech in the face of climate change-related precipitation reduction? New Phytol. 210: 443–458. DOI: 10.1111/nph.13798.

Schweingruber FH. 2007. Wood structure and environment. Springer Verlag, Berlin, Germany.

Sperry JS, Meinzer FC, McCulloh KA. 2008. Safety and efficiency conflicts in hydraulic architecture: scaling from tissues to trees. Plant Cell Environ. 31: 632–645. DOI: 10.1111/j.1365-3040.2007.01765.x.

Trifilò P, Raimondo F, Lo Gullo MA, Barbera PM, Salleo S, Nardini A. 2014. Relax and refill: xylem rehydration prior to hydraulic measurements favors embolism repair in stems and generates artificially low PLC values. Plant Cell Environ. 37: 2491–2499. DOI: 10.1111/pce.12313.

Tyree MT, Davis SD, Cochard H. 1994. Biophysical perspectives of xylem evolution: is there a tradeoff of hydraulic efficiency for vulnerability to dysfunction? IAWA J. 15(4): 335–360.

Tyree MT, Zimmermann MH. 2002. Xylem structure and the ascent of sap. Springer Verlag, Berlin, Germany.

von Arx G, Crivellaro A, Prendin AL, Čufar K, Carrer M. 2016. Quantitative wood anatomy — practical guidelines. Front. Plant Sci.: 7. DOI: 10.3389/fpls.2016.00781.
von Arx G, Kueffer C, Fonti P. 2013. Quantifying plasticity in vessel grouping — added value from the image analysis tool ROXAS. IAWA J. 34: 433–454. DOI: 10.1163/22941932-00000035.
West GB, Brown JH, Enquist BJ. 1999. A general model for the structure and allometry of plant vascular systems. Nature 400: 664–667. DOI: 10.1038/23251.
Wheeler JK, Sperry JS, Hacke UG, Hoang N. 2005. Inter-vessel pitting and cavitation in woody Rosaceae and other vesselled plants: a basis for a safety versus efficiency trade-off in xylem transport. Plant Cell Environ. 28: 800–812. DOI: 10.1111/j.1365-3040.2005.01330.x.
Zimmermann MH, Jeje AA. 1981. Vessel-length distribution in stems of some American woody plants. Can. J. Bot. 59: 1882–1892.

Edited by Shuichi Noshiro

APPENDIX

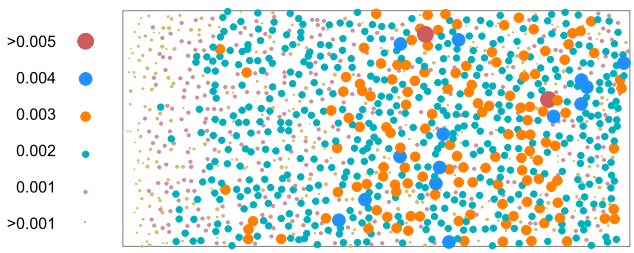

Figure A1. Example of the steps applied for the spatial analysis of a stem cross-section of *Fagus sylvatica* L. Cross-sectional digital image used for binary acquisition and point determination. The legend displays the area of measured vessels in mm².

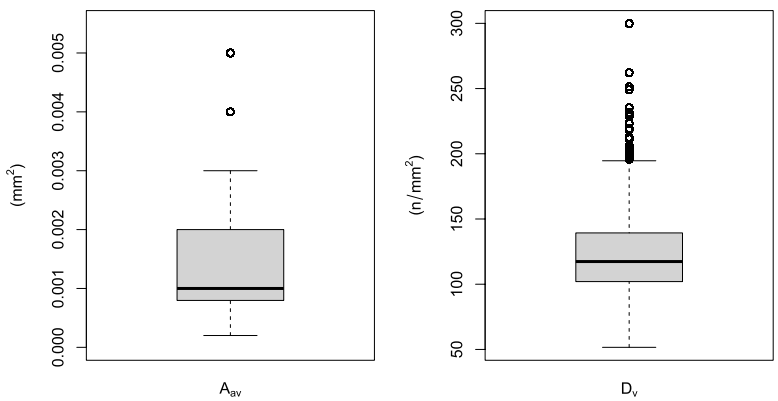

Figure A2. Boxplots of measured xylem conduit area (A_{av}) and conduit density (D_v) (left and right panel, respectively). Each box represents the 75th to 25th percentiles, the bold line shows the median, upper and lower marks are the largest to smallest observation values which are less than or equal to the upper and lower quartiles plus 1.5 times the length of the interquartile range. Measured conduit area range from 0.0002007 to 0.0055 mm², while conduit density ranges from 51.6164 to 299.8446 n/mm².

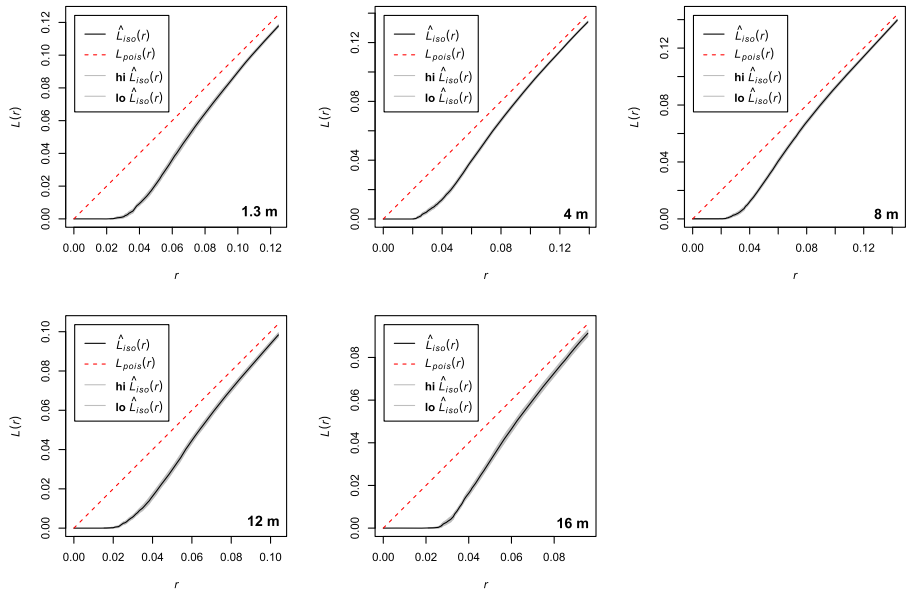

Figure A3. Application of a Ripley function in the form of the *L*-function related to the distance from the ring boundary (r, mm). Full line is the observed value for the data pattern, dashed red line theoretical value of $L(r)$ for CSR, shadows are upper and lower critical boundary for simulated 95% confidence envelopes of $L(r)$.

Table A1.
Linear mixed-effect models of nearest neighbour distance (NN_d) as a function of cambial age (CA), tree-ring width (TRW) and distance from the stem base (m).

	NNd		
	Est.	std. Beta	*P*-value
Predictor			
(Intercept)	0.06		***
CA	0.00	0.19	***
TRW	0.00	0.46	***
Hf 4	−0.00	−0.63	***
Hf 8	−0.01	−0.85	***
Hf 12	−0.01	−1.66	***
Hf 16	−0.01	−1.56	***
Random effects			
ICC	0.43		
N_{id}	8		
Obs	1047		
R_m^2/R_c^2	0.516/0.716		

Est, estimates; std. Beta, standardized estimates; ICC, Intraclass Correlation; N_{id}, sampling ID; Obs: number of observations; R^2_m = marginal *R*-square (proportion of variance explained by fixed factors); R^2_c = conditional *R*-square (proportion of variance explained by fixed and random factors).

*** Statistically significant at $P < 0.001$.